1994

Theoretical Analysis of the Discharge Performance of a NiOOH/ H_2 Cell

Z. Mao
University of South Carolina - Columbia

P. De Vidts
University of South Carolina - Columbia

Ralph E. White
University of South Carolina - Columbia, white@cec.sc.edu

John Newman
University of California - Berkeley

Publication Info

Journal of the Electrochemical Society, 1994, pages 54-64.

Publisher's link: http://dx.doi.org/10.1149/1.2054710
DOI: 10.1149/1.2054710

Theoretical Analysis of the Discharge Performance of a $NiOOH/H_2$ Cell

Z. Mao,* P. De Vidts, and R. E. White*

Department of Chemical Engineering, University of South Carolina, Columbia, South Carolina 29208

John Newman*

Department of Chemical Engineering, University of California, Berkeley, California 94720

ABSTRACT

A mathematical model is presented for the discharge of a $NiOOH/H_2$ cell. This model includes diffusion and migration in the electrolyte phase as well as proton diffusion and ohmic drop across the solid active material in the porous nickel electrode. A theoretical analysis of the cell performance is presented for different design parameters using this model. It is predicted that proton diffusion in the solid active material is the main factor in limiting the cell voltage and the utilization of the active material. It is also predicted that use of a thick nickel electrode is an effective method for increasing electrode capacity per unit area. This model can be used to predict the two-discharge-plateau behavior of a nickel electrode.

Mathematical modeling of porous nickel electrodes in an alkaline solution has been the subject of many research projects for various applications such as NiOOH/Zn, NiOOH/Cd, and $NiOOH/H_2$ batteries. Based on a macrohomogeneous approach and on the assumption that transport processes in the $NiOOH/Ni(OH)_2$ active material in nickel electrodes are much faster than those in the electrolyte phase, Choi and Yao developed a one-dimensional mathematical model for porous nickel electrodes in a zincate alkaline solution.[1] They found that the porosity or active material loading has little effect on the utilization of the active material in a porous nickel electrode and that the material utilization is approximately inversely proportional to the electrode thickness because of the limitation of the mass transport in the electrolyte phase. Micka and Rousar[2,3] developed a one-dimensional model similar to that of Choi and Yao, but they included the dependence of the transport properties on the electrolyte concentration and the dependence of the conductivity of the solid material on the composition of the active material. They investigated the effect of the position of the current collector in the nickel electrode on the charge and discharge behavior and found that the position of the current collector is of little importance. Fan and White[4,5] proposed a similar model for NiOOH/Cd batteries. Their model includes oxygen evolution on charge and uses a non-Nernst expression for the equilibrium potential of the nickel electrode. Contrary to the findings of Choi and Yao, Fan and White found that the mass-transport processes in the electrolyte phase have little effect on the electrode behavior and that the charge and discharge behavior is kinetically controlled. They also claimed that electrodes with uniform material loading perform better than those with nonuniform material distribution. Unfortunately, discrepancies exist between experimental observations and predictions from these models. Specifically, the predicted electrode potentials are higher and flatter than experimental data, and the predicted utilization of the active material in the nickel electrode is nearly 100% and is nearly independent of discharge rate, which differs from experimental data in that the measured utilization decreases with an increase in the discharge rate.

Many investigations[6-8] have presented experimental work that indicates that proton diffusion and ohmic drop in the solid active material are the major factors that limit nickel-electrode behavior. Sinha[9] developed a comprehensive model of porous nickel electrodes in which the solid active material was treated as a semiconductor film covering the nickel substrate and the transport processes in the solid phase were described using semiconductor theory. Unfortunately, his model contains many parameters that cannot be obtained experimentally. Consequently, meaningful simulations of electrode behavior with his model were carried out only for cases so simplified that the model became similar to the previous one-dimensional models. Bouet *et al.*[10] presented a discharge model which includes proton diffusion in the solid active material in a macrohomogeneous model similar to the models described above. They showed that their model predictions are in excellent agreement with their experimental data. They also showed that a relationship exists between the utilization of the active material in the nickel electrode, discharge rate, and electrode thickness. Evidently, the inclusion of proton diffusion in the solid phase is a significant improvement in the simulation of a porous nickel electrode. However, it appears that further improvement may be achieved if both proton diffusion and the ohmic drop across the active material in the nickel electrode were to be included in their model.

The models described above except for the one by Fan and White[4,5] are mainly for a single electrode. Mao and White[11] showed recently that a single TiS_2 electrode immersed in a large volume of electrolyte behaves much differently from that in a cell with a thin separator. To simulate realistically the behavior of a nickel electrode in a battery, the interactions among the electrode, separator, and the counterelectrode should be included.

The work presented here is a mathematical model for the discharge of a $NiOOH/H_2$ cell. This model includes the features of the aforementioned models, and it includes both proton diffusion and ohmic drop across the solid active material in a porous nickel electrode, concentration and potential variations in the separator, and the effect of electrolyte concentration on the polarization of the hydrogen electrode during discharge.

Development of the Mathematical Model

General description.—When a $NiOOH/H_2$ cell is discharged, nickel oxyhydroxide is electrochemically reduced to nickel hydroxide at the surface of the $NiOOH/Ni(OH)_2$ in the porous nickel electrode. The reaction is generally expressed as

$$NiOOH + H_2O + e^- \rightarrow Ni(OH)_2 + OH^- \qquad [1]$$

Proton diffusion into the bulk of the solid phase makes it possible for this reaction to continue at the active material surface.[8,12,13] In this reaction, water is consumed and hydroxide ions are generated. Therefore, there is an increase in the alkaline concentration in the electrode during discharge, resulting in a concentration polarization to reaction 1. If the proton diffusion into the bulk solid phase is a slow process, $Ni(OH)_2$ builds up on the surface of the $NiOOH/Ni(OH)_2$ active material, which causes a significant

* Electrochemical Society Active Member.

rise in the polarization for reaction 1. Since pure $Ni(OH)_2$ is essentially an electrical insulator (the actual electrode material may have a higher conductivity than $Ni(OH)_2$ because it contains some amount of cobalt hydroxide), an appreciable ohmic drop exists across the active-material layer, particularly at low states of charge.

The overall resistance of the nickel electrode therefore includes five components: (*i*) the concentration polarization due to a rise in KOH concentration in the electrode; (*ii*) a potential drop in the electrolyte; (*iii*) the activation polarization of the electrochemical reaction; (*iv*) the polarization due to the $Ni(OH)_2$ buildup on the NiOOH/ $Ni(OH)_2$ surface; and (*v*) the ohmic drop across the solid phase in the electrode. All these polarizations change when the electrode design parameters such as the active-material loading level, electrode thickness, and electrolyte concentration are changed. The mathematical model presented here includes all these effects.

The separator in a $NiOOH/H_2$ cell separates the nickel electrode from the hydrogen electrode and serves as a conduit for mass transport and ionic charge conduction between the two electrodes. The resistance of this region includes the mass-transfer resistance and the potential drop across the region. However, its thickness also affects transport processes in the nickel electrode.

The electrochemical reaction at the hydrogen electrode is the oxidation of hydrogen during discharge, generally expressed as

$$\frac{1}{2}H_2 + OH^- \rightarrow H_2O + e^- \qquad [2]$$

This reaction consumes both hydrogen and hydroxyl ions, causing a decrease in the electrolyte concentration in and near the hydrogen electrode. This decrease in the electrolyte concentration results in an increased hydrogen solubility in the electrolyte because hydrogen solubility decreases exponentially with electrolyte concentration,[14] and consequently, leads to a reduction in the concentration polarization for the reaction. The equilibrium potential for the hydrogen electrode shifts in the positive direction due to the decreasing hydrogen pressure and the decreasing OH^- concentration during discharge. These two factors affect the electrochemical behavior of the hydrogen electrode.

Model equations.—Figure 1 presents a schematic diagram of the cell. The nickel electrode substrate is a porous sinter nickel plaque. The active material is impregnated into the substrate. Based on the macrohomogeneous approach and concentrated binary solution theory developed by Newman *et al.*,[15,16] the equation for the mass balance for potassium hydroxide in the electrolyte phase has been derived by previous researchers.[2,4,9,10] When convection is neglected as suggested by Sinha[9] and Fan[17] because its effect is small compared to diffusion and migration, the mass-balance equation becomes

$$\epsilon\frac{\partial c}{\partial t} = -\frac{\partial}{\partial x}\left[-D\epsilon^{\tau}\frac{\partial c}{\partial x} - \frac{t_-}{F}i\right] - \frac{j}{F} \qquad [3]$$

where c and D represent the concentration of potassium hydroxide and its diffusion coefficient, t_- is the transference number of hydroxide ions, ϵ represents the electrode porosity which is assumed here to be uniform because its effect is insignificant as reported by Sinha[9] and Fan,[17] and the symbol i represents the current density in the electrolyte phase, which can be expressed by a modified Ohm's law[2,15]

$$i = -\kappa\left\{\frac{\partial\Phi}{\partial x} + \frac{2RT}{F}\left[(1-t_-) + \frac{c}{2c_o}\right]\frac{\partial}{\partial x}\ln cf_{\pm}\right\} \qquad [4]$$

where κ represents the effective conductivity of the electrolyte in the porous nickel electrode, c_o is water concentration in mol/cm^3, and $f_{\pm}$ represents the mean molar activity coefficient of the electrolyte. A Hg/HgO reference electrode in the same solution was chosen in deriving Eq. 4.

According to charge conservation, the local transfer current per unit volume of the electrode must be equal to the rate of change in the current density in the electrolyte phase

$$\frac{\partial i}{\partial x} = j \qquad [5]$$

It is assumed here that oxygen evolution/reduction and hydrogen oxidation at the nickel electrode are negligible compared to the reduction of NiOOH to $Ni(OH)_2$ during discharge; consequently, the transfer current j is equal to the faradaic current due to reaction 1 or the diffusion rate of protons into the bulk phase of the solid active material at the surface of the $NiOOH/Ni(OH)_2$

$$j = -aFD_s\left.\frac{\partial c_s}{\partial y}\right|_{y=\delta} \qquad [6]$$

where a represents the electrochemically active surface area per unit volume and c_s and D_s represent the proton concentration and its diffusion coefficient in the solid phase, respectively.

Substitution of Eq. 5 and 6 into Eq. 3 and substitution of Eq. 4 and 6 into Eq. 5 yield the final two equations for the KOH concentraiton and the potential in the electrolyte as follows

$$\epsilon\frac{\partial c}{\partial t} = \epsilon^{\tau}\left[\frac{\partial D}{\partial x}\frac{\partial c}{\partial x} + D\frac{\partial^2 c}{\partial x^2}\right] - a(t_- - 1)D_s\left.\frac{\partial c_s}{\partial y}\right|_{y=\delta} \qquad [7]$$

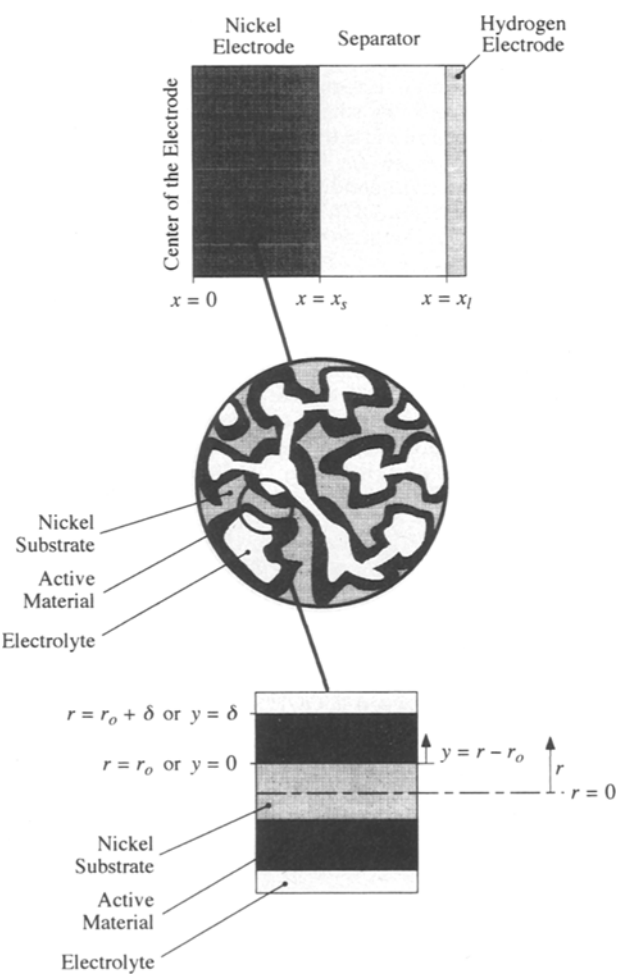

Fig. 1. Schematic diagram of the $NiOOH/H_2$ cell. Top, the cell and its components; center, internal structure of the porous nickel electrode; bottom, idealization of a point in the solid phase of the nickel electrode as a cylinder of nickel substrate surrounded by a layer of active material.

$$-\frac{\partial \kappa}{\partial x}\left\{\frac{\partial \Phi}{\partial x}+\frac{2RT}{F}\left[(1-t_-)+\frac{c}{2c_o}\right]\frac{\partial}{\partial x}\ln cf_\pm\right\}$$

$$-\kappa\left\{\frac{\partial^2\Phi}{\partial x^2}+\frac{2RT}{F}\left[(1-t_-)+\frac{c}{2c_o}\right]\frac{\partial^2}{\partial x^2}\ln cf_\pm\right.$$

$$\left.+\frac{RT}{F}\frac{\partial}{\partial x}\left(\frac{c}{c_o}\right)\frac{\partial}{\partial x}\ln cf_\pm\right\}=-aFD_s\left.\frac{\partial c_s}{\partial y}\right|_{y=\delta} \quad [8]$$

At the surface of the $NiOOH/Ni(OH)_2$ ($y = \delta$), the local diffusion rate of protons into the bulk solid is equal to the local electrochemical reaction rate, which may be expressed by a Butler-Volmer equation. This equality can be expressed as

$$-FD_s\left.\frac{\partial c_s}{\partial y}\right|_{y=\delta}=i_{c,o}\left\{\exp\left[\frac{\alpha F}{RT}\eta_c\right]-\exp\left[-\frac{(1-\alpha)F}{RT}\eta_c\right]\right\} \quad [9]$$

where

$$\eta_c=\Phi_1-\Phi-\Phi_{c,eq} \quad [9a]$$

$$\Phi_{c,eq}=\Phi^*_{c,eq}+\frac{RT}{F}\left[b\ln\frac{c_t-c_s}{c_s}+d\left(\frac{c_s}{c_t}-0.5\right)\right] \quad [9b]$$

$$i_{c,o}=i_{c,ref}\left(\frac{c_s}{c_{s,ref}}\right)\left(\frac{c}{c_{ref}}\right)\exp\left[\frac{\alpha F}{RT}(\Phi_{c,eq}-\Phi_{c,ref})\right] \quad [9c]$$

Φ_1 represents the potential in the solid active material, $\Phi_{c,eq}$ is the equilibrium potential for the NiOOH electrode, and $\Phi^*_{c,eq}$ is the equilibrium potential for the NiOOH electrode evaluated at 50% state of charge, and its dependence on the electrolyte concentration is presented in Appendix B. The symbol c_t represents the proton concentration in the solid phase when the active material is completely discharged. Equivalently, c_t can be thought of as the concentration of nickel hydroxide according to Lubovtsev and Slaidin.[13] Such an equivalence has been used to determine the proton diffusion coefficient by some investigators.[3,6,10] It is assumed here that Ohm's law dictates the potential distribution in the solid phase; *i.e.*, electron transfer is the only mode for the electrical conduction in the solid phase even though the $NiOOH/Ni(OH)_2$ may be a semiconductor;[18,19] consequently, the following equation is assumed to be valid at the interface

$$\sigma\left.\frac{\partial \Phi_1}{\partial y}\right|_{y=\delta}=FD_s\left.\frac{\partial c_s}{\partial y}\right|_{y=\delta} \quad [10]$$

If nickel substrate particles are treated as equivalent cylindrical particles of average radius r_o and the active material of average thickness δ is on these cylindrical particles, then proton diffusion in the solid phase in the radial direction may be described by Fick's law in cylindrical coordinates

$$\frac{\partial c_s}{\partial t}=\frac{\partial D_s}{\partial y}\frac{\partial c_s}{\partial y}+D_s\left[\frac{1}{y+r_o}\frac{\partial c_s}{\partial y}+\frac{\partial^2 c_s}{\partial y^2}\right] \quad [11]$$

The proton diffusion in the axial direction is neglected here because the thickness of the active-material film (δ) is small compared to the electrode thickness (x_s). Since it is assumed that proton diffusion occurs simultaneously with electron transfer between NiOOH and $Ni(OH)_2$ in the solid phase, no net charge is generated or consumed in the bulk active material phase; thus, the divergence of the current density should be zero

$$\frac{\partial \sigma}{\partial y}\frac{\partial \Phi_1}{\partial y}+\sigma\left[\frac{\partial^2\Phi_1}{\partial y^2}+\frac{1}{y+r_o}\frac{\partial \Phi_1}{\partial y}\right]=0 \quad [12]$$

At the interface between the $NiOOH/Ni(OH)_2$ and the nickel substrate ($y = 0$), the flux of protons must be zero

$$-D_s\left.\frac{\partial c_s}{\partial y}\right|_{y=0}=0 \quad [13]$$

Also, the potential in the active layer should be equal to that in the substrate at this interface

$$\Phi_1|_{y=0}=\Phi_c \quad [14]$$

where Φ_c represents the potential in the substrate which is assumed here to be a constant throughout the electrode because the conductivity of the substrate is large compared to that of the $NiOOH/Ni(OH)_2$ layer and it does not change during discharge, and also because the porous substrate is three dimensional in structure and current can flow in any direction.

Equations 7-8 and 11-12 form a complete set of equations describing the mass transport and the electrical field distributions in the porous nickel electrode. The boundary conditions for Eq. 11-12 have been given by Eq. 9-10 at $y = \delta$ and by Eq. 13-14 at $y = 0$. The boundary conditions for Eq. 7-8 are discussed next. At the back side of the nickel electrode ($x = 0$), the flux of hydroxide ions is zero due to symmetry, and the current density in the electrolyte phase vanishes at this boundary. At the interface between the nickel electrode and the separator ($x = x_s$), the flux of hydroxide ions and the current density in the electrolyte phase evaluated from the nickel electrode side are equal to those evaluated from the separator. These boundary conditions after rearrangement are

$$\left.\frac{\partial c}{\partial x}\right|_{x=0}=0 \quad [15]$$

$$\left.\frac{\partial \Phi}{\partial x}\right|_{x=0}=0 \quad [16]$$

$$\epsilon^\tau\left.\frac{\partial c}{\partial x}\right|_{x=x_s^-}=\epsilon_s^\tau\left.\frac{\partial c}{\partial x}\right|_{x=x_s^+} \quad [17]$$

$$\kappa\left.\frac{\partial \Phi}{\partial x}\right|_{x=x_s^-}=\kappa\left.\frac{\partial \Phi}{\partial x}\right|_{x=x_s^+} \quad [18]$$

The transport equations for the separator region are identical to Eq. 7 and 8 except they do not contain the terms due to reaction 1 and the porosity of the separator is used in these equations.

Since the discharge capability of a hydrogen electrode in a $NiOOH/H_2$ cell is much higher than that of a nickel electrode, a hydrogen electrode is treated here as a flat plate electrode. Its electrochemical behavior is assumed to be described by using a modified Butler-Volmer equation

$$i_a=i_{a,o}\left\{\exp\left[\frac{\beta F}{RT}\eta_a\right]-\exp\left[-\frac{(1-\beta)F}{RT}\eta_a\right]\right\} \quad [19]$$

where

$$\eta_a=\Phi_a-\Phi-\Phi_{a,eq} \quad [19a]$$

$$\Phi_{a,eq}=\Phi^o_{a,eq}-\frac{RT}{2F}\ln P \quad [19b]$$

$$i_{a,o}=i_{a,ref}\left(\frac{c_{H_2}}{c_{H_2,ref}}\right)^{(1-\beta)}\left(\frac{c}{c_{ref}}\right)^{2-\beta} \quad [19c]$$

The dissolved hydrogen concentration c_{H_2} is assumed to be related to its concentration at the interface between the electrolyte and the hydrogen gas phase, $c^s_{H_2}$

$$\frac{c_{H_2}}{c^s_{H_2}}=\left(1-\frac{i_a}{i_l}\right) \quad [20]$$

where i_l is the limiting current density under the same hydrogen pressure. It is assumed that the dissolved hydrogen concentration at the gas/electrolyte interface is in equilibrium with hydrogen gas and that Henry's law is valid. Consequently, $c^s_{H_2}$ can be correlated with the electrolyte concentration at the hydrogen electrode and hydrogen pressure P as

$$c^s_{H_2}=c^o_{H_2}P\exp(-Kc) \quad [21]$$

where $c^o_{H_2}$ represents the dissolved hydrogen concentration in pure water under a hydrogen pressure of 1 atm at 298.15 K. The limiting current density can be expressed by the equation

$$i_l=i_{l,ref}\left(\frac{P}{P_{ref}}\right)\exp\left[-K(c-c_{ref})\right] \quad [22]$$

Substitution of Eq. 20-22 into Eq. 19 yields the final form of the kinetic expression for the hydrogen electrode reaction

$$i_a = i_{a,ref}\left[\frac{P}{P_{ref}}\exp\left(-K(c-c_{ref})\right) - \frac{i_a}{i_{l,ref}}\right]^{1-\beta}\left(\frac{c}{c_{ref}}\right)^{2-\beta} \times\left\{\exp\left[\frac{\beta F}{RT}\eta_a\right] - \exp\left[-\frac{(1-\beta)F}{RT}\eta_a\right]\right\} \quad [23]$$

The hydrogen pressure in the NiOOH/H_2 cell decreases proportionally to the passed charge during discharge

$$P = P^0 + \frac{A}{V}RT\frac{i_{app}t}{2F} \quad [24]$$

where P^0 is the initial hydrogen pressure, i_{app} represents the applied current density based on the geometric area of the electrode, which is chosen to be negative for discharge mode, A is the total geometric electrode area, and V is the total volume of hydrogen gas in the cell. To avoid using V, which may not be measured easily, the following correlation can be used

$$\frac{A}{V}RT = \frac{2(P^0 - P_\infty)}{(c_t - c_s^\circ)(\epsilon_o - \epsilon)x_s} \quad [25]$$

where the symbol P_∞ represents the residual hydrogen pressure or precharge pressure.

There are three equations at the hydrogen electrode that can be used to complete the discharge model. Two of these equations can be used as the boundary conditions, and the third one is used to determine the potential of the hydrogen electrode. These equations are (*i*) the flux of hydroxide ions is equal to the equivalence of the discharge current density at this electrode; (*ii*) the current density in the electrolyte phase is equal to the applied discharge current density; and (*iii*) the current density due to the hydrogen oxidation is equal to the applied discharge current density. These equations are

$$-D\epsilon_s^\tau\frac{\partial c}{\partial x} - \frac{t_-}{F}i_{app} = -\frac{i_{app}}{F} \quad [26]$$

$$i = -\kappa\left\{\frac{\partial\Phi}{\partial x} + \frac{2RT}{F}\left((1-t_-) + \frac{c}{2c_o}\right)\frac{\partial}{\partial x}\ln cf_\pm\right\} = i_{app} \quad [27]$$

$$-i_{app} = i_{a,ref}\left[\left(\frac{P^0}{P_{ref}} + \frac{i_{app}t}{F}\frac{\frac{P^0}{P_{ref}} - \frac{P_\infty}{P_{ref}}}{(c_t - c_s^\circ)(\epsilon_o - \epsilon)x_s}\right)\exp\left[-K(c-c_{ref})\right] + \frac{i_{app}}{i_{l,ref}}\right]^{1-\beta} \times\left(\frac{c}{c_{ref}}\right)^{2-\beta}\left\{\exp\left[\frac{\beta F}{RT}\eta_a\right] - \exp\left[-\frac{(1-\beta)F}{RT}\eta_a\right]\right\} \quad [28]$$

Equation 28 was obtained by substituting Eq. 25 and 24 into Eq. 23 with $i_a = i_{app}$.

Thus, the discharge model for a NiOOH/H_2 cell consists of the transport Eq. 7-8 for the electrolyte phase in the porous nickel electrode, two equations similar to Eq. 7-8 for the separator, and Eq. 11-12 for the solid NiOOH/$Ni(OH)_2$ phase in the nickel electrode. The boundary conditions are Eq. 9-10 and Eq. 13-14 for the solid phase in the nickel electrode, and Eq. 15-18 and Eq. 26-28 for the electrolyte phase. The initial distributions of the electrolyte concentration and the proton concentration in the NiOOH/$Ni(OH)_2$ solid phase in the nickel electrode are needed to solve these equations. It is assumed here that the concentration of potassium hydroxide and the proton concentration in the solid phase are uniform throughout the cell before a discharge current is applied, *i.e.*

$$c|_{t=0} = c^\circ \quad [29]$$

$$c_s|_{t=0} = c_s^\circ \quad [30]$$

Numerical Procedure

A finite-difference method was used to solve the model equations. The first step in the numerical procedure was to write the differential equations in finite-difference form using three-point and central finite differences as approximations of first- and second-order derivatives in the space coordinate and using the Crank-Nicolson approximation. The resulting nonlinear coupled algebraic equations were then solved using a Newton-Raphson method implemented into the algorithm recently developed by Mao and White.[20] The fixed input parameters are listed in Appendix A, and the auxiliary functions (D, κ, c/c_o, $f_\pm$, and $\Phi^*_{c,eq}$ as functions of the electrolyte concentration and σ as a function of the state of charge) are given in Appendix B. Appendix C presents the correlation between the active-material loading and surface area per unit volume for an ideal situation. The results presented next were obtained using 71 node points in the x-direction and 51 node points in the y-direction and a time step $Q_t/|i_{app}| \times 10^{-3}$ s where Q_t is the total theoretical electrode capacity per unit area.

Since a measured cell voltage is a relative value between the nickel oxyhydroxide and the hydrogen electrodes in the cell, the potential of one electrode can be chosen arbitrarily; the potential of the other electrode is then obtained by solving the model equations for a given discharge current density. Here, the potential in the substrate of the nickel electrode (Φ_o) was chosen arbitrarily to be equal to $\Phi_{c,ref}$, and the trial values for the potential in the solid active material (Φ_1), the potential in the electrolyte phase (Φ), and the hydrogen electrode potential (Φ_a) were set equal to the values obtained at the previous time step. The trial values for Φ_1 at the first time step were determined as follows

$$\Phi_1 = \Phi_{c,ref} - \frac{i_{app}}{\sigma a}y \quad 0 \le x \le x_s, \quad 0 < y \le \delta \quad [31]$$

where σ is determined from Eq. B-5 with $c_s = c_s^\circ$. A constant trial value was used for the potential in the electrolyte in the nickel oxyhydroxide electrode (Φ) at the first time step and was obtained by solving the following equation

$$\frac{i_{app}}{ax_s} = i_{c,o}\left\{\exp\left[\frac{\alpha F}{RT}\left(\Phi_1(\delta) - \Phi - \Phi_{c,eq}\right)\right] - \exp\left[-\frac{(1-\alpha)F}{RT}\left(\Phi_1(\delta) - \Phi - \Phi_{c,eq}\right)\right]\right\} \quad [32]$$

Trial values for Φ in the separator were calculated

$$\Phi(x) = \Phi(x_s) - \frac{x - x_s}{\kappa_s}i_{app}, \quad x_s < x \le x_1 \quad [33]$$

A trial value for the anode potential (Φ_a) was obtained by solving Eq. 28 at $t = 0$.

Results and Discussion

Figure 2 presents predicted discharge curves at different discharge rates. These predicted curves are qualitatively consistent with experimental observations. That is, the cell voltage decreases with discharge time, and the utilization of the active material in the nickel electrode decreases with an increase in discharge rate. At the beginning of discharge, these predicted cell voltages appear to change more rapidly than experimental curves reported in the literature. Because of oxygen evolution on a NiOOH electrode in these high states of charge, the experimental cells actually may start at a slightly less charged state than assumed here (99% of full charge). Therefore, the predicted discharge curves given here should be compared to experimental observation except for the initial part of the discharge curve (less than 5% of the electrode capacity).

The cell voltage drop during discharge consists of potential losses in the NiOOH and the hydrogen electrodes and ohmic loss across the separator. Figure 3 shows each predicted component for the 10 C rate discharge shown in Fig. 2. The overpotential for the hydrogen electrode ($\Phi_a - \Phi(x_1) - \Phi_{a,eq}$) decreases slightly in the early stages of discharge and then increases with time. The initial decrease is

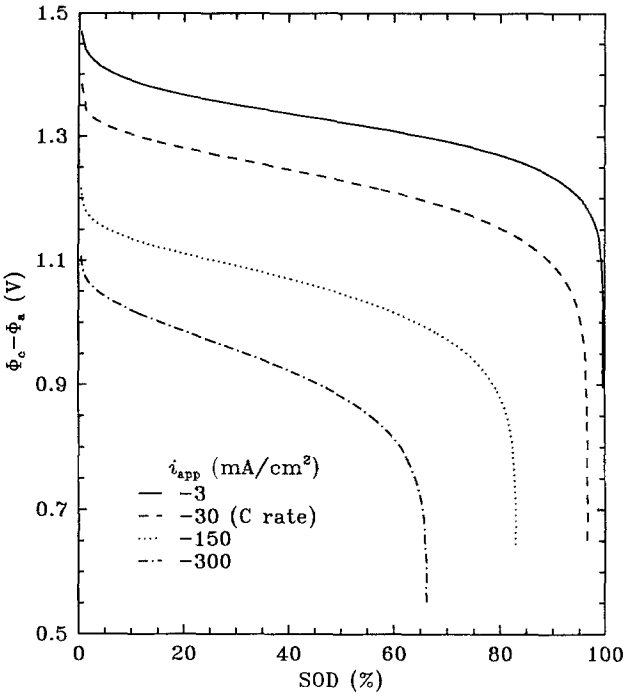

Fig. 2. Predicted discharge curves at different discharge rates. The state of discharge (SOD) was calculated using the equation: SOD = $|i_{app}|t/Q_t \times 100$.

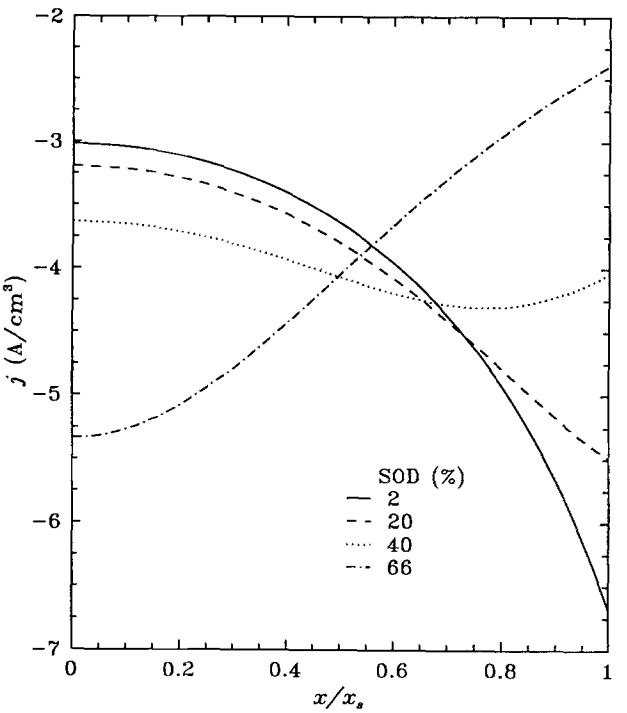

Fig. 4. The transfer current per unit volume as a function of position in the nickel electrode at different states of discharge. i_{app} = −300 mA/cm^2 (10 C rate).

due to an increase in the hydrogen solubility caused by the decrease in the concentration of KOH in the hydrogen electrode. After that, the increase in the overpotential is due mainly to the equilibrium-potential shift in the positive direction as the hydrogen pressure decreases with discharge time. Also, the ohmic drop across the separator increases slightly during discharge, as shown in Fig. 3, because the electrolyte concentration in the separator decreases during discharge, as discussed later, resulting in a decrease in the electrolyte conductivity in this region. The overall overpotential for the nickel electrode ($\Phi_c - \Phi(x_s) - \Phi_{c,eq}$) consists of the ohmic drop across the active material in the electrode ($\Phi_1(\delta) - \Phi_c$), the potential drop in the electrolyte phase ($\Phi(x_s) - \Phi(0)$), and the concentration polarization due to an $Ni(OH)_2$ buildup on the surface of the active material and due to an increase in the electrolyte concentration within the electrode. All these potential loss components increase during discharge, but their contributions to the overall overpotential of this electrode are significantly different, as discussed next.

Figures 4, 5, and 6 present the transfer current per unit volume, the electrolyte concentration, and the potential in

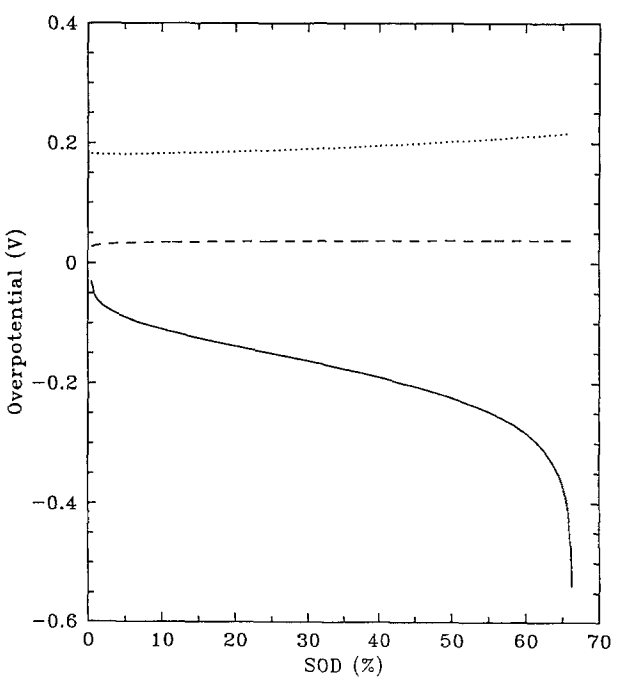

Fig. 3. Predicted potential loss at the cathode, across the separator, and at the hydrogen electrode during discharge for i_{app} = −300 mA/cm^2 (10 C rate). Curves are: (—) $\Phi_c - \Phi(x_s) - \Phi_{c,eq}$; (- - -) $\Phi(x_l) - \Phi(x_s)$; and (· · ·) $\Phi_a - \Phi(x_l) - \Phi_{a,eq}$.

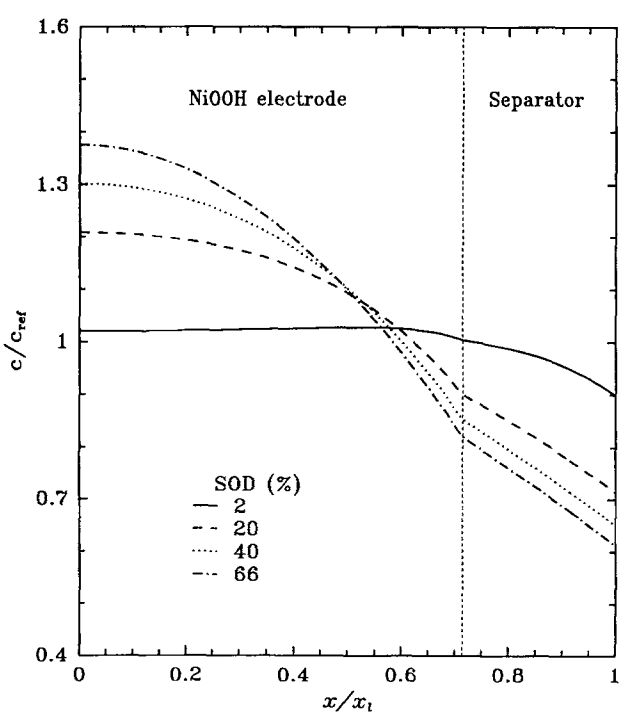

Fig. 5. The electrolyte concentration profiles at different states of discharge during discharge. i_{app} = −300 mA/cm^2 (10 C rate).

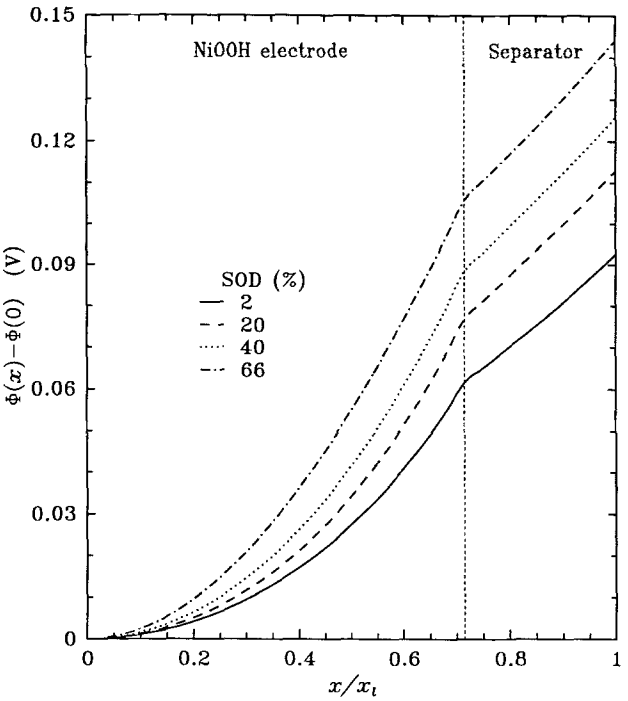

Fig. 6. The distribution of the potential in the electrolyte phase at different states of discharge. i_{app} = −300 mA/cm² (10 C rate).

the electrolyte phase as a function of the position perpendicular to the electrode surface at different states of discharge for a 10 C rate discharge. Figure 4 shows that the charge transfer occurs predominantly in the front side of the nickel electrode near the separator during the early stages of discharge, and gradually penetrates into the electrode as the discharge proceeds, and finally it occurs mainly in the region near the back side of the electrode. As expected, the concentration of the electrolyte increases continuously with time in the region near the back side of the porous NiOOH electrode during discharge; however, it first increases and then decreases in the region toward the separator and decreases continuously in the separator, as shown in Fig. 5. The potential drop in the electrolyte phase within the NiOOH electrode increases significantly in time because of the penetration of the reaction into the electrode, but the potential drop across the separator changes slightly, as shown in Fig. 6.

The variations in c, Φ, and the transfer current as functions of position and time during discharge are strongly related to one another. The higher potential in the electrolyte phase near the separator yields a greater driving force for the electrochemical reduction of NiOOH to $Ni(OH)_2$ in this region during the early part of discharge, causing a higher reaction rate, and consequently, an increase in the electrolyte concentration in this region. As $Ni(OH)_2$ accumulates on the surface of the active material because of slow proton diffusion into the bulk solid phase, the equilibrium potential for the nickel reaction shifts in the negative direction, reducing the driving force for the reaction. Consequently, the reaction rate decreases gradually in the region near the separator and increases farther into the nickel electrode. Consumption of OH^- ions in the hydrogen electrode ($x = x_1$) during discharge results in a decrease in the electrolyte concentration in the separator and also in the nickel electrode near the separator, as shown in Fig. 5. Figure 6 shows that use of a thin separator yields a higher cell voltage and possibly a greater utilization of the active material in the NiOOH electrode by reducing the ohmic drop and the transport resistance through the separator.

Figure 7 presents the potential distribution in the solid phase in the nickel electrode at the end of discharge. The potential in the solid phase drops sharply near the surface of the active material because of the substantial decrease of the electronic conductivity in the region, but it is uniform in the x-direction, and the total magnitude of the potential drop is small compared to the overall potential drop for the nickel electrode. The conductivity of the solid active material is 2.51×10^{-5} S/cm calculated from Eq. B-5 in Appendix B when the active material is completely discharged. Since the solid active material is thin (δ = 1.5 μm calculated using Eq. C-6) and the electrode has a large surface area ($a = 4.0 \times 10^3$ cm²/cm³ calculated using Eq. C-7 in Appendix C), the current density across the active material is small, and consequently, there is only a small potential drop across the solid active material even at the end of discharge. However, if the conductivity of the completely discharged material becomes as low as 10^{-12} S/cm, as given by Barnard,[21] the potential drop across the active material is significant.

Figures 8a and b show the distributions for $Ni(OH)_2$ in both directions perpendicular to the active material surface (y) and to the projected electrode suface (x) at an early stage of discharge (2%) and at the end of discharge (62%) for the 10 C rate case shown in Fig. 2. The nickel hydroxide concentration sharply increases toward the active-material surface ($y = \delta$) and toward the separator ($x = x_s$) when the cell begins to be discharged, and it becomes almost saturated along the surface of the active material ($y = \delta$) throughout the nickel electrode at the end of discharge. This accumulation of $Ni(OH)_2$ on the surface of the solid active material and the associated ohmic drop across it may cause the premature drop of the cell voltage under the given discharge rate. When the discharge rate is reduced, the $Ni(OH)_2$ accumulation on the surface is slowed by proton diffusion into the bulk solid phase, and consequently, more active material can be discharged.

Although proton diffusion in the $NiOOH/Ni(OH)_2$ solid material has been investigated extensively, the reported values for the proton diffusion coefficient range from 10^{-6} to 10^{-13} cm²/s.[6,8,12,13,22] It is generally accepted that the proton diffusion coefficient depends on the crystalline structure of the active material[8] and on the level of hydration.[23] Therefore, the method used to prepare a nickel electrode, aging, and charge/discharge cycling all affect the cell performance. Figure 9 illustrates how the value of the proton

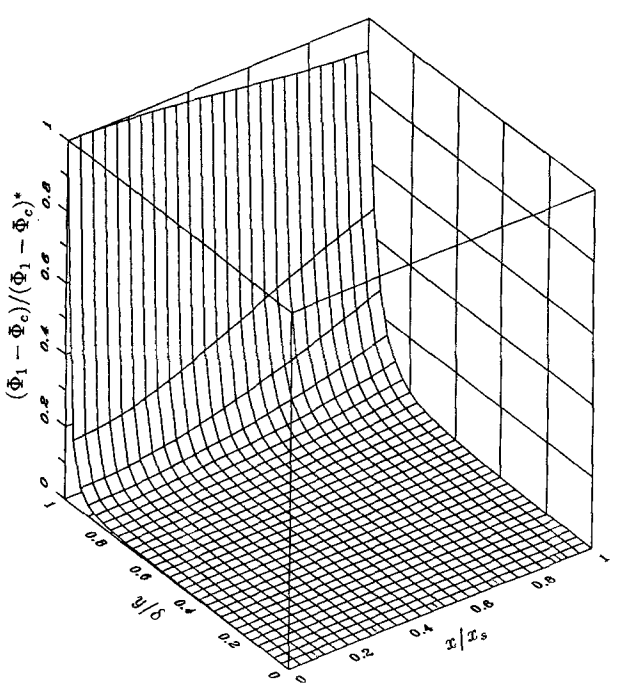

Fig. 7. The potential distribution across the solid active material and along the NiOOH electrode at the end of discharge. $(\Phi_1 - \Phi_c)^*$ = 0.2206 mV, i_{app} = −300 mA/cm² (10 C rate).

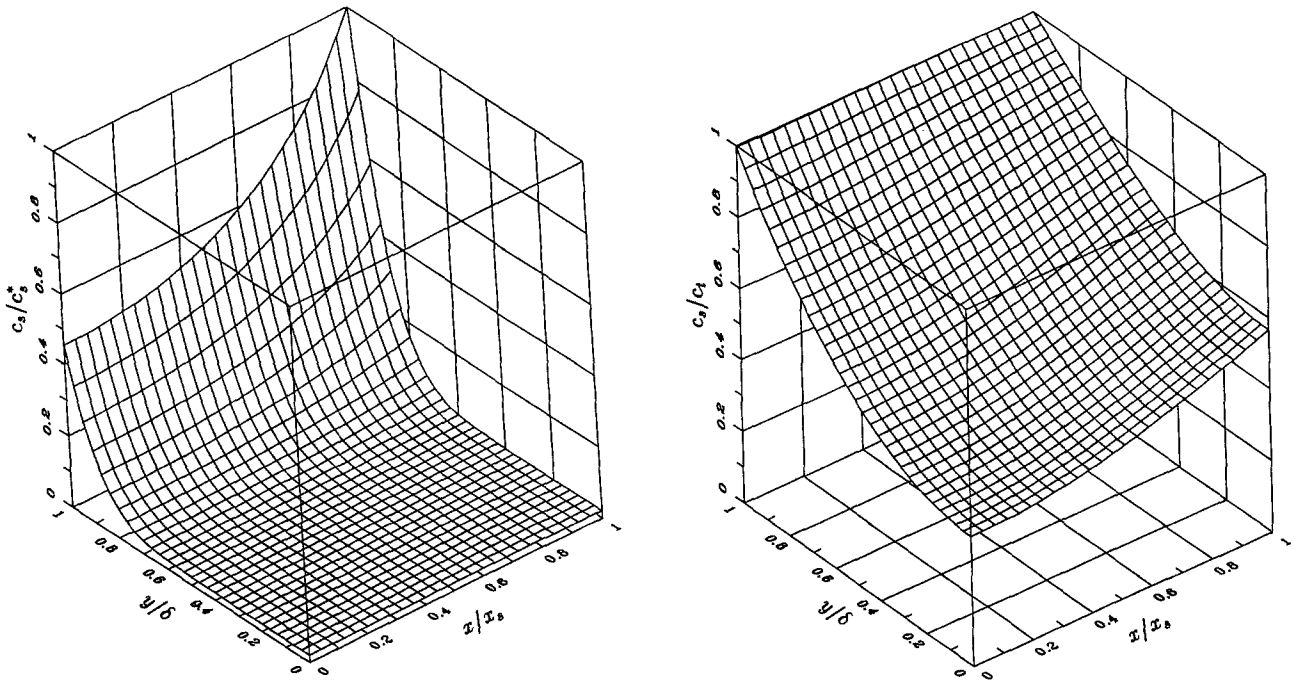

Fig. 8. The distribution of $Ni(OH)_2$ in the active material phase in the nickel electrode at two states of discharge. (a) 2%, $c_s^* = 0.2399c_i$; (b) 62%; $i_{app} = -300$ mA/cm^2 (10 C rate).

diffusion coefficient affects the cell voltage and the utilization of the active material in a NiOOH electrode. As expected, a small proton diffusion coefficient results in both a lower cell voltage and less utilization of the active material. For the conditions used in Fig. 9, the active material in the nickel electrode can be fully discharged if the proton diffusion coefficient is greater than 10^{-10} cm^2/s, but only a small portion of it can be utilized if the proton diffusion coefficient is smaller than 10^{-12} cm^2/s.

Effect of electrode thickness.—Figure 10 presents the predicted deliverable capacity relative to the theoretical capacity as a function of the electrode thickness at two constant discharge rates of −30 and −150 mA/cm^2. The material utilization increases with the electrode thickness for thin electrodes at both the high and low discharge rates because the particles are unable to absorb the protons fast enough for thin electrodes. For the high rate discharge, the material utilization reaches a maximum and decreases with further increases in the electrode thickness because mass transport and ohmic drop in the electrolyte become limiting. These phenomena are similar to those leading to Fig. 5 by West *et al.*[24] Thus there may exist an optimum electrode thickness for a high rate of discharge, and use of

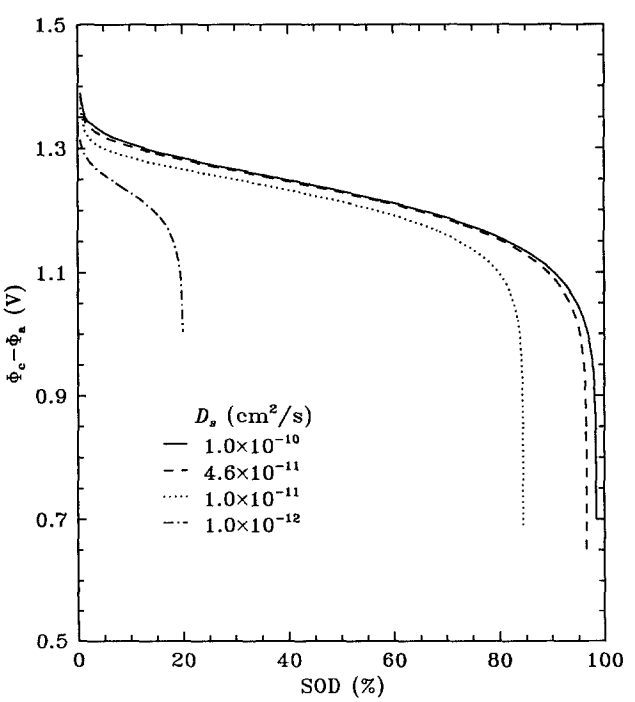

Fig. 9. The sensitivity of the discharge cell voltage and the active material utilization to proton diffusion coefficient. $i_{app} = -300$ mA/cm^2 (10 C rate).

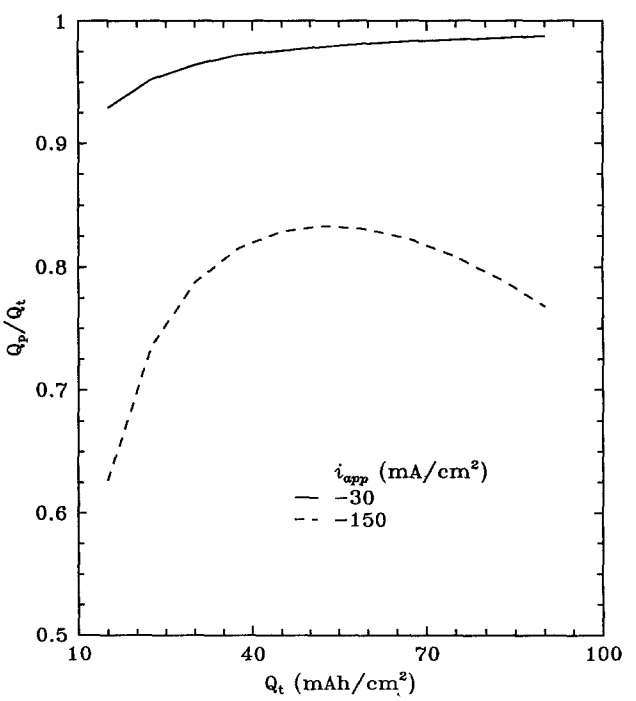

Fig. 10. Predicted effect of electrode thickness on the utilization of the active material in the NiOOH electrode at two discharge rates. $Q_p = i_{app}t_e/Q_t$, where t_e is the time to the end of discharge (*i.e.*, at 0.9 V), and $Q_t = Q_{t,o}x_s$ where $Q_{t,o} = 400$ mAh/cm^3.

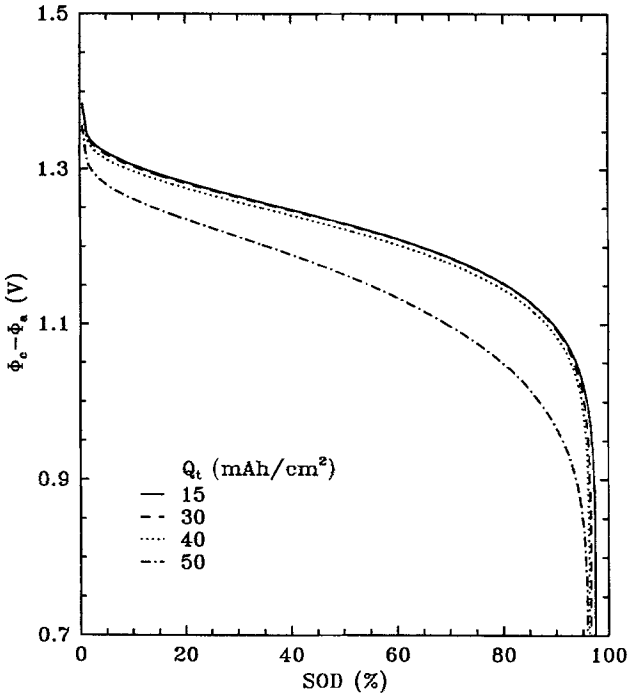

Fig. 11. Predicted discharge curves for electrodes with different active material loading. The active material loading is altered by changing Q_t for a given x_s. This changes both ϵ (see Eq. A-2) and δ (see Eq. C-6).

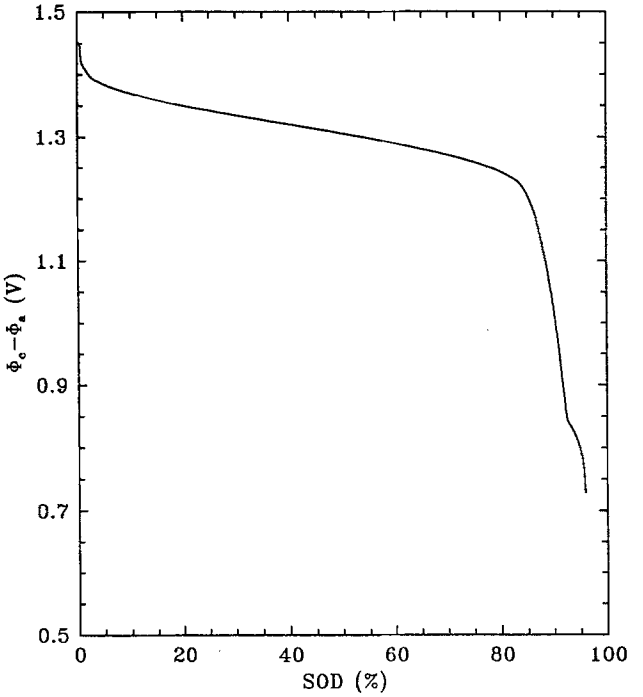

Fig. 12. Predicted discharge curve with σ given by Eq. 34. i_{app} = −6 mA/cm^2 (C/5 rate), and $D_s = 1.0 \times 10^{-11}$ cm^2/s.

a thick electrode for a low rate of discharge may result in higher material utilization.

It is desirable to impregnate nickel hydroxide as much as possible into sintered nickel electrodes for a high volumetric energy density. When more nickel hydroxide is loaded into a sinter electrode, the interfacial area tends to increase; however, the porosity of the electrode decreases, and the distance for proton diffusion in the solid phase becomes longer (*i.e.*, δ is greater). These factors may cause an increase in the concentration polarization. Therefore, there may be a limit for material loading per unit volume. Figure 11 presents predicted discharge curves for different material loadings at a discharge current density of −30 mA/cm^2. The discharge curves are almost the same for the electrodes with a theoretical capacity loading less than 40 mAh/cm^2; however, the one with 50 mAh/cm^2 deviates significantly from the others, indicating that the limitation of mass transport and ohmic drop in the electrolyte phase overcomes the beneficial effect of a large surface area. The correlation between the material loading and the electrode interfacial area presented in Appendix C is for an ideal situation, it may overestimate the surface area because there is some overlapping areas in an actual electrode which are neglected in the ideal case. By comparing the two methods used in obtaining a high capacity per unit separator area or unit volume, as illustrated in Fig. 10 and 11, use of thick electrodes appears more flexible and more practical than loading more material per unit volume.

Second discharge plateau.—It is often reported that discharge curves have two plateaus for a NiOOH electrode when the electrode is discharged at a small rate. The second plateau appears at a potential at least 300 mV more negative than the first one depending on the discharge current density. Recent work suggests that the second plateau is due to formation of an insulating film at the NiOOH/substrate interface[7,25] or a depletion layer at the $Ni(OH)_2$/electrolyte interface,[21,26] instead of being due to intrinsically less active material as suggested in earlier work.[27,28] Zimmerman[29] suggested that an insulating film may form at the interface between the active material and the electrolyte; the effect of such a film should be the same as he suggested earlier.[25] The prediction of the potential profile in the solid active material given in Fig. 7 indicates that the mathematical model presented here may be used to predict the two-plateau behavior of a NiOOH electrode if the correct expression is used for the conductivity of the solid active material. Figure 12 presents a predicted discharge curve when the following equations are used for the conductivity of the solid active material

$$\sigma = \begin{cases} 0.1185 \exp\left[-24.45(c_s/c_t)^4\right] & 0 \le c_s \le 0.9c_t \\ 0.1185 \exp\left[-24.45 \times (0.9)^4\right] & c_s \ge 0.9c_t \end{cases} \quad [34]$$

The shape of the predicted discharge curve is the same qualitatively as experimental observations reported in the literature.[25] Here, as shown in Eq. 34, the conductivity of the solid active material decreases steadily with time during discharge until a certain point where it becomes constant. Correspondingly, the potential drop across the active material increases by *ca.* 300 mV when the $Ni(OH)_2$ builds up on the surface of the NiOOH/$Ni(OH)_2$ to the point where its resistance rises sharply. After this, the discharge continues at the lower potential until the surface of the active material becomes completely saturated with $Ni(OH)_2$.

Conclusions

A mathematical model for discharge of a NiOOH/H_2 cell has been presented. Theoretical analysis of the cell performance has been carried out for different design parameters using this model. It was concluded that the transport process in the solid active material, *i.e.*, proton diffusion, is the main factor in determining the cell voltage and the utilization of the active material. Also, the use of a thick NiOOH electrode is an effective method for increasing electrode capacity per unit separator area. The model can be used to predict the two-discharge-plateau behavior of a nickel electrode.

Acknowledgments

The authors are grateful for the financial support for this work from the Office of Research and Development, the Hughes Aircraft Company, and the NASA Center for Space Power at Texas A&M University. Participation of Dr. Deyuan Fan, now at the Shell Westhollow Research Center, in the early stage of this work is acknowledged. Valuable discussions with Mr. Paul Timmerman of the Jet Propulsion Laboratory are appreciated. The authors are also grateful

for computer time on the Cray-YMP supercomputer at Texas A&M University from Cray Research, Inc.

Manuscript submitted Sept. 8, 1992; revised manuscript received Sept. 21, 1993.

The University of South Carolina assisted in meeting the publication costs of this article.

APPENDIX A
Fixed Input Parameters

Symbol	Parameter	Ref.
a	4.036×10^3 cm^2/cm^3 (calculated using Eq. C-7 in Appendix C)	
a_o	2.0×10^3 cm^2/cm^3	
b	1	
c^o	5.8×10^{-3} mol/cm^3	
$c^o_{H_2}$	1.9202×10^{-7} mol/cm^3	
c_{ref}	5.8×10^{-3} mol/cm^3	
$c_{s,ref}$	$0.5c_t$ mol/cm^3	
c^o_s	$10^{-3}c_t$ mol/cm^3	
c_t	3.238×10^{-2} mol/cm^3 (calculated using Eq. A-1 given below)	
D_s	4.6×10^{-11} cm^2/s	12
d	0	
$i_{c,ref}$	2.0×10^{-4} A/cm^2	
$i_{a,ref}$	3.5×10^{-4} A/cm^2	30
$i_{l,ref}$	5.0 A/cm^2	
K	315.4 cm^3/mol	31
M	105 g/mol	32
x_s	0.075 cm	
$x_l - x_s$	0.03 cm	
P^0	50 atm	
P_{ref}	50 atm	
P_∞	1.5 atm	
Q_t	108 C/cm^2 (30×10^{-3} Ah/cm^2)	
r_o	1.5×10^{-4} cm (calculated using Eq. C-1 in Appendix C)	
T	298 K	
ϵ	0.389 (calculated using Eq. A-2)	
ϵ_o	0.85	
ϵ_s	0.65	
$\Phi^o_{a,eq}$	−0.926 V	33
$\Phi_{c,ref}$	$\Phi_{c,eq}$ at $c_s = c_{s,ref}$ and $c = c_{ref}$	
α	0.5	
β	0.5	
δ	1.527×10^{-4} cm (calculated using Eq. C-6 in Appendix C)	
τ	1.5	
ρ	3.4 g/cm^3 (calculated using the rule of mixtures over pure $Ni(OH)_2$ and H_2O)	

$$c_t = \frac{\rho}{M} \qquad [A\text{-}1]$$

$$\epsilon = \epsilon_o - \frac{Q_t}{F}\frac{M}{\rho}\frac{1}{x_s} \qquad [A\text{-}2]$$

APPENDIX B
Auxiliary Functions

The parameters D, $f_\pm$, κ, c/c_o, and $\Phi^*_{c,eq}$ are functions of the electrolyte concentration c (in mol/cm^3). Correlations for these parameters were obtained by using nonlinear least squares regression of polynomial or nearly polynomial functions to experimental data reported in literature. The IMSL subroutine UNLSF was used in these curve fittings. The resulting functions are listed as follows.

D. Electrolyte diffusion coefficient

$$D = 2.625 \times 10^{-5} + 1.3347 \times 10^{-3}c - 5.0759c^{2.5711} \text{ cm}^2/\text{s} \qquad [B\text{-}1]$$

The experimental concentrations used in this regression range from 0.10×10^{-3} to 10.4×10^{-3} mol/cm^3 and are from Ref. 34. The average relative error was *ca.* 0.68%.

c/c_o. The ratio of electrolyte to water concentration

$$\frac{c}{c_o} = 18.119c + 1.1259 \times 10^2c^2 + 2.3273 \times 10^4c^3 \qquad [B\text{-}2]$$

The experimental concentrations range from 0.0 to 13.45×10^{-3} mol/cm^3 for the regression of Eq. B-2 and are from Table 8.1 of Ref. 35. The average values of the data for 20 and 30°C were used here. The average error was about 0.10%.

$f_\pm$. Molar activity coefficient of electrolyte

$$f_\pm = 7.757 \times 10^{-1} - 94.499c + 6.1237 \times 10^4c^2 + 6.4598 \times 10^5c^3 \exp(2.4719 \times 10^2c) \qquad [B\text{-}3]$$

The range of the experimental data for the regression of Eq. B-3 is $0.10 \times 10^{-3} \sim 12.16 \times 10^{-3}$ mol/cm^3; they are from Table A-2 of Ref. 36. The average relative error was *ca.* 3.38%.

κ. Specific conductivity of the free electrolyte

$$\kappa_o = -7.593 \times 10^{-5} + 2.3831 \times 10^2c - 2.5997 \times 10^4c^2 + 7.6442 \times 10^5c^3 - 9.6275c^4 \text{ S/cm} \qquad [B\text{-}4]$$

The effective electrolyte conductivities in the nickel electrode and in the separator were estimated using the equation, $\kappa = \kappa_o\epsilon^\tau$ and $\kappa_s = \kappa_o\epsilon_s^\tau$, where κ_o represents the conductivity of the free KOH electrolyte. The experimental data range for the regression of Eq. B-4 is $1.25 \times 10^{-6} \sim 12.75 \times 10^{-3}$ mol/cm^3, and are from Ref. 35 and also from Table A-3 of Ref. 36. The average error was *ca.* 6.02%.

σ. Specific conductivity of the $NiOOH/Ni(OH)_2$ active material

$$\sigma = 0.1185 \exp\left[-8.459\left(\frac{c_s}{c_t}\right)^4\right] \text{ S/cm} \qquad [B\text{-}5]$$

This correlation between the conductivity of the $NiOOH/Ni(OH)_2$ active material and the state of charge is from Ref. 2.

$\Phi^*_{c,eq}$. The equilibrium potential for a NiOOH electrode at 50% of state-of-charge *vs.* a Hg/HgO reference electrode

$$\Phi^*_{c,eq} = 3.1797 \times 10^{-1} - 1.5868 \times 10^{-2} \ln cf_\pm - 9.4705 \times 10^{-4}(\ln cf_\pm)^2 - 3.7995 \times 10^{-5}(\ln cf_\pm)^3 \text{ V} \qquad [B\text{-}6]$$

The experimental data for the regression of Eq. B-6 range from 7.0×10^{-4} to 14.7×10^{-3} mol/cm^3. They are from Fig. 2 in Ref. 37. In retrospect, we should have used their Fig. 6 and their Eq. 2 for which they conclude a different stoichiometry from that used in our reaction 1. Thus, extrapolation of Eq. B-6 should not be attempted.

APPENDIX C
Relations among Specific Surface Area, Porosity, and Thickness of the $NiOOH/Ni(OH)_2$ Layer

When more active material is impregnated into a porous nickel electrode, the porosity of the electrode decreases whereas the interfacial area of the electrode tends to increase. To predict the effect of material loading on the discharge behavior, these changes must be taken into account. The following approximation was used in the model.

Assuming that the specific surface area of the nickel substrate a_o and its porosity ϵ_o are known, and that the nickel substrate consists of numerous cylindrical particles that have an equivalent radius r_o, the relation between the specific surface area, the porosity, and the radius may be expressed as

$$a_o = \frac{2(1 - \epsilon_o)}{r_o} \qquad [C\text{-}1]$$

The specific surface area can be expressed as

$$a_o = 2n\pi r_o L \qquad [C\text{-}2]$$

where n represents the number of cylindrical particles per unit volume and L is the length of each cylinder. A volume balance gives the relations between the porosity and the radius

$$1 - \epsilon_o = \pi n r_o^2 L \qquad [C\text{-}3]$$

For a nickel electrode with $NiOOH/Ni(OH)_2$ loaded, its porosity becomes ϵ, assuming that the thin $NiOOH/Ni(OH)_2$ layer is on the external surface of the Ni cylinders, the following volume balance is valid

$$\epsilon_o - \epsilon = \frac{a_o}{2r_o}(r^2 - r_o^2) \qquad [C\text{-}4]$$

The radius r can be obtained from this equation as

$$r = \sqrt{r_o^2 + \frac{2r_o(\epsilon_o - \epsilon)}{a_o}} = r_o\sqrt{\frac{1 - \epsilon}{1 - \epsilon_o}} \qquad [C\text{-}5]$$

The average thickness of the active material in the nickel electrode is estimated as

$$\delta = r - r_o = r_o \left[\sqrt{\frac{1-\epsilon}{1-\epsilon_o}} - 1 \right] \qquad [C\text{-}6]$$

and the specific surface area becomes

$$a = \frac{1-\epsilon}{1-\epsilon_o} \frac{r_o}{r} a_o = \sqrt{\frac{1-\epsilon}{1-\epsilon_o}}\, a_o \qquad [C\text{-}7]$$

Alternatively, one may assume that the active material is on the inside surfaces of hollow cylinders as treated by Dunning.[38]

LIST OF SYMBOLS

- A total geometric electrode surface area in a NiOOH/H_2, cm^2
- a surface area per unit volume of the NiOOH electrode, cm^2/cm^3
- a_o surface area per unit volume of the nickel substrate, cm^2/cm^3
- b constant in Eq. 9b
- c electrolyte concentration, mol/cm^3
- c_{H_2} dissolved hydrogen concentration, mol/cm^3
- $c^o_{H_2}$ the dissolved hydrogen concentration in pure water under a pressure of 1 atm, mol/cm^3
- $c^s_{H_2}$ dissolved hydrogen concentration at the electrolyte/gas interface, mol/cm^3
- c^o initial electrolyte concentration, mol/cm^3
- c_{ref} reference electrolyte concentration, mol/cm^3
- c_o water concentration, mol/cm^3
- c_s proton concentration in the NiOOH/$Ni(OH)_2$ solid phase, mol/cm^3
- $c_{s,ref}$ reference proton concentration in the solid phase, mol/cm^3
- c^o_s initial proton concentration in the solid phase, mol/cm^3
- c_t total proton concentration in the solid phase, mol/cm^3
- D diffusion coefficient of potassium hydroxide, cm^2/s
- D_s proton diffusion coefficient in the solid phase, cm^2/s
- d constant in Eq. 9b
- F Faraday constant, 96,487 C/mol
- $f_\pm$ mean molar activity coefficient of electrolyte
- i_{app} discharge current density, A/cm^2
- i current density in the electrolyte phase, A/cm^2
- i_a current density due to hydrogen oxidation at the anode, A/cm^2
- i_l limiting current density of hydrogen oxidation at the anode, A/cm^2
- $i_{l,ref}$ limiting current density of hydrogen oxidation at the anode under reference hydrogen pressure and reference electrolyte concentration, A/cm^2
- $i_{a,o}$ exchange current density for the hydrogen oxidation at the anode, A/cm^2
- $i_{a,ref}$ exchange current density for the hydrogen oxidation at the anode evaluated at a reference state, A/cm^2
- $i_{c,o}$ exchange current density for the nickel electrode reaction, A/cm^2
- $i_{c,ref}$ exchange current density for the nickel electrode reaction evaluated at a reference state, A/cm^2
- j transfer current per unit volume of the nickel electrode, A/cm^3
- K concentration-effect constant, cm^3/mol
- M molecular weight of hydrated nickel hydroxide ($Ni(OH)_2 \cdot 2/3\ H_2O$), g/mol
- P hydrogen pressure, atm
- P^0 initial hydrogen pressure, atm
- P_{ref} reference hydrogen pressure, atm
- P_∞ residual or precharge hydrogen pressure, atm
- Q_p utilization of the active material in the NiOOH electrode
- Q_t total charge in the nickel electrode per projected area of the electrode, C/cm^2
- $Q_{t,o}$ charge in the nickel electrode per unit volume of the electrode, C/cm^3
- R universal gas constant, 8.3143 J/K · mol
- r_o equivalent radius of nickel substrate particles, cm
- T temperature, K
- t time, s
- t_- transference number of hydroxyl ions
- V effective volume of hydrogen gas in a NiOOH/H_2 cell, cm^3
- x spatial coordinate in the direction normal to the electrode surface, cm
- x_s thickness of the NiOOH electrode, cm
- x_l total thickness of the cell, cm
- y spatial coordinate in the direction normal to the surface of the NiOOH/$Ni(OH)_2$, cm

Greek

- α transfer coefficient of the nickel electrode reaction
- β transfer coefficient of the anode reaction
- ϵ porosity of the nickel electrode
- ϵ_o porosity of the nickel substrate
- ϵ_s porosity of the separator
- τ porosity and tortuosity effect constant
- κ effective electrolyte conductivity, S/cm
- κ_s effective electrolyte conductivity in the separator, S/cm
- Φ potential in electrolyte phase, V
- Φ_a hydrogen electrode potential, V
- $\Phi_{a,eq}$ equilibrium hydrogen electrode potential, V
- $\Phi^0_{a,eq}$ standard equilibrium hydrogen potential *vs.* Hg/HgO, V
- Φ_1 potential in the solid active-material phase in the nickel electrode, V
- Φ_c potential in the nickel substrate, V
- $\Phi_{c,eq}$ equilibrium nickel electrode potential, V
- $\Phi_{c,ref}$ $\Phi_{c,eq}$ evaluated at $c = c_{ref}$ and $c_s = c_{s,ref}$, V
- $\Phi^*_{c,eq}$ equilibrium NiOOH electrode potential evaluated at 50% state of charge *vs.* Hg/HgO, V
- ρ density of hydrated nickel hydroxide ($Ni(OH)_2$ 2/3 H_2O), g/cm^3
- η_a overpotential at the hydrogen electrode as expressed by Eq. 19a, V
- η_c local overpotential in the NiOOH electrode as expressed by Eq. 9a, V
- σ conductivity of the solid NiOOH/$Ni(OH)_2$ phase, S/cm

REFERENCES

1. K. W. Choi and N. P. Yao, in *Battery Design and Optimization,* S. Gross, Editor, PV 79-1, p. 63, Electrochemical Society Proceedings Series, Princeton, NJ (1979).
2. K. Micka and I. Rousar, *Electrochim. Acta,* **25,** 1085 (1980).
3. K. Micka and I. Rousar, *ibid.,* **27,** 765 (1982).
4. D. Fan and R. E. White, *This Journal,* **38,** 17 (1991).
5. D. Fan and R. E. White, *ibid.,* **38,** 2952 (1991).
6. C. Zhang and S-M. Park, *ibid.,* **134,** 2966 (1987).
7. A. H. Zimmerman and P. K. Effa, *ibid.,* **131,** 709 (1984).
8. G. W. D. Briggs and P. R. Snodin, *Electrochim. Acta,* **27,** 565 (1982).
9. M. Sinha, Ph.D. Thesis, University of California, Los Angeles, CA (1982).
10. J. Bouet, F. Richard, and Ph. Blanchard, in *Proceedings of the Symposium on Nickel Hydroxide Electrodes,* D. A. Corrigan and A. H. Zimmerman, Editors, PV 90-4, p. 260, The Electrochemical Society Proceedings Series, Pennington, NJ (1990).
11. Z. Mao and R. E. White, *J. Power Sources,* **43,** 181 (1993).
12. D. M. MacArthur, *This Journal,* **117,** 729 (1970).
13. P. D. Lukovtsev and G. J. Slaidin, *Electrochim. Acta,* **6,** 17 (1962).
14. R. Battino and E. Wilhelm, *IUPAC Solubility Data Series,* Vol. 5/6, p. 1, C. L. Young, Editor, Pergamon Press, New York (1980).
15. J. Newman and W. Tiedemann, *AIChE J.,* **21,** 25 (1975).
16. J. S. Newman, *Electrochemical Systems,* 2nd ed., p. 454, Prentice Hall, Englewood Cliffs, NJ (1991).
17. D. Fan, Ph.D. Thesis, Texas A&M University, College Station, TX (1991).
18. B. Klapste, J. Mrha, K. Micka, J. Jindra, and V. Maracek, *J. Power Sources,* **4,** 349 (1979).
19. B. Klapste, K. Micka, J. Mrha, and J. Vondrak, *ibid.,* **8,** 352 (1982).
20. Z. Mao and R. E. White, *This Journal,* To be published.
21. R. Barnard, C. F. Randell, and F. L. Tye, *J. Appl. Electrochem.,* **10,** 127 (1980).
22. G. Davolio and E. Soragni, *Electrochim. Acta,* **28,** 335 (1983).
23. V. A. Volynskii and Yu. N. Chernykh, *Elektrokhimiya,* **13,** 1070 (1977).
24. K. West, T. Jacobsen, and S. Atlung, *This Journal,* **129,** 1480 (1982).
25. A. H. Zimmerman, in *Proceedings of the Symposium on*

Nickel Hydroxide Electrodes, D. A. Corrigan and A. H. Zimmerman, Editors, PV 90-4, p. 311, Electrochemical Society Proceedings Series, Pennington, NJ (1990).
26. R. Barnard, G. T. Crickmore, J. A. Lee, and F. L. Tye, *J. Appl. Electrochem.*, **10**, 61 (1980).
27. S. E. S. El Wakkard and E. S. Emara, *J. Chem. Soc.*, **4**, 3504 (1953).
28. J. Besson, *Ann. Chim.*, **2**, 527 (1947).
29. A. H. Zimmerman, Private communication, January, 1992.
30. B. V. Tilak, P. W. T. Lu, J. E. Colman, and S. Srinivasan, in *Comprehensive Treatise of Electrochemistry*, J. O'M. Bockris, B. E. Conway, E. Yeager, and R. E. White, Editors, Vol. 2, p. 1, Plenum Press, New York (1984).
31. R. Battino and E. Wilhelm, *IUPAC Solubility Data Series*, C. L. Young, Editor, Vol. 5/6, p. 1, Pergamon Press, New York (1980).
32. D. M. MacArthur, *This Journal*, **117**, 422 (1970).
33. S. G. Bratsch, *J. Phys. Chem. Ref. Data*, **18**, 1 (1989).
34. R. N. Bhatia, K. E. Gubbins, and R. D. Walker, in *Handbook of Electrolyte Solutions*, Part A, p. 1085, V. M. M. Lobo, Editor, Elsevier, New York (1989).
35. D. Bennion, Ph.D. Thesis, University of California, Berkeley, CA (1964).
36. S. Uno Falk and A. J. Salkind, *Alkaline Storage Batteries*, p. 577, John Wiley & Sons, Inc., New York (1969).
37. P. L. Bourgault and B. E. Conway, *Can. J. Chem.*, **38**, 1557 (1960).
38. J. S. Dunning, Ph.D. Thesis, University of California, Los Angeles, CA (1971).

Electrochromic Oxidation and Reduction of Cobalt and Zinc Naphthalocyanine Thin Films

Hisao Yanagi* and Masahiro Toriida

Faculty of Engineering, Kobe University, Rokkodai, Nada, Kobe 657, Japan

ABSTRACT

Electrochromism of cobalt and zinc naphthalocyanines (CoNc, ZnNc) was investigated in thin films vacuum-deposited on indium tin oxide substrates. The CoNc film exhibited color changes from original green to purple both upon reduction and oxidation, and the ZnNc film exhibited a color change from green to brown only upon oxidation. The electrochromic reduction was a reversible process depending on an electroactivity of the central Co metal, and the electrochromism was attributed to a transition from a reduced state related to the Co(I) center to a π^*-state of the Nc-ligand. On the other hand, the electrochromic oxidation irreversibly occurred at the Nc-ring ligand. The ring-oxidation was stably maintained by a retention of incorporated anions, which caused a film restructuring accompanied with a discorder of molecular stacking from the original α-polymorphic form to an amorphous structure in the oxidized state.

Metal naphthalocyanines (MNc's, Fig. 1), which are chemically modified analogues of metal phthalocyanines (MPc's), exhibit a strong absorption in the long-wavelength region (700 to 900 nm) because of the large π-electron conjugating macrocyclic structure.[1-4] The spectral properties of MNc's have attracted interests in their applications to optical data recording and display materials.[5,6] For constructing practical devices MNc's can be processed into thin films by a vacuum-deposition technique.[7] Previous papers[8-13] have reported crystal growth and molecular orientation of MNc thin films vacuum-deposited on different substrates. In the thin films MNc molecules crystallize in a columnar stack similar to that in vacuum-deposited MPc films.[14,15] The electronic structure of MNc's in solid state is significantly influenced by their molecular stacking modes,[7] as expected from an analogy to MPc's.[16,17] Furthermore, the extended benzoannulation in MNc's, as compared to MPc's, causes a change in their electronic energy states. The energy level of both occupied and unoccupied states of MNc's is higher than that of MPc's because of the larger conjugated π-electron system. This electronic potential change influences their electrical, electrochemical, and photoelectrochemical behavior.[18,19]

As is known, MPc's exhibit electrochromic reduction and/or oxidation, and their electrochromism has been intensively studied for rare-earth metal diphthalocyanines.[20-24] For example, lutetium diphthalocyanine [$LuH(Pc)_2$] shows multicolor changes from green to red upon oxidation[20] and from green to violet upon reduction.[22] These electrochromic reactions occur with migration of anions and cations, respectively, from electrolyte solutions into the $LuH(Pc)_2$ films to compensate charges. Ordinary single-ring MPc's like CoPc and ZnPc also exhibit electrochromic oxidation.[24,25] It has been reported that the oxidation is a reversible one-electron process for ZnPc,[25] while CoPc undergoes two-oxidation processes, the first of which is quasi-reversible and the second is irreversible.[24] It has been revealed that cyclic oxidations and rereductions of ZnNc indicate a gradual loss of consumed charges which is caused by a film restructuring.[25] In the case of CoPc a metal oxidation of the central Co has also been speculated for the second oxidation.[24] Thus, an electroactivity of the coordinated metals in Pc ligands significantly influences their electrochromic behavior.

As well as the coordinated metals, characteristics of macrocyclic ligands have an affect on their electrochemical activities. In general, MNc's are expected to be easily oxidized due to their extended π-electron macrocyclic system, as compared to MPc's. In this respect the Nc ligand system arouses interests in their photoelectrochemical and electrochromic properties. However, only a few reports have been made on electrochromism of MNc's, so far. Shimura *et al.*[26] described a cathodic electrochromism of CoNc films. The vacuum-deposited CoNc film showed a color change from green to red upon reduction in a deaerated aqueous electrolyte, and this electrochromism was speculated in terms of metal to ligand charge transfer (MLCT),[27] *i.e.*, transition from a reduced state of the Co center to an excited π^*-state of the Nc-ligand.

In this work, in order to clarify the electrochromism of MNc's, electrochromic reactions both upon reduction and oxidation were investigated for CoNc and ZnNc thin films vacuum-deposited on an indium-tin oxide (ITO) conductive glass substrate. Cyclic voltammetry and visible (VIS) spectroscopy demonstrate a reversible electrochromic reduction for CoNc and irreversible electrochromic oxidation for both CoNc and ZnNc. The oxidized film was very stable in air, so that chemical and structural changes upon the electrochromic oxidation were examined by x-ray pho-

* Electrochemical Society Active Member.